The RELAMPAGO Lightning Mapping Array: Overview and Initial Comparison with the Geostationary Lightning Mapper

TIMOTHY J. LANG,[a] ELDO E. ÁVILA,[b] RICHARD J. BLAKESLEE,[a] JEFF BURCHFIELD,[c] MATTHEW WINGO,[c] PHILLIP M. BITZER,[c] LAWRENCE D. CAREY,[c] WIEBKE DEIERLING,[d] STEVEN J. GOODMAN,[e] BRUNO LISBOA MEDINA,[c] GREGORY MELO,[f] AND RODOLFO G. PEREYRA[b]

[a] *NASA Marshall Space Flight Center, Huntsville, Alabama*
[b] *Facultad de Matemática, Astronomía y Física, Universidad Nacional de Córdoba, Córdoba, Argentina*
[c] *University of Alabama in Huntsville, Huntsville, Alabama*
[d] *University of Colorado Boulder, Boulder, Colorado*
[e] *Thunderbolt Global Analytics, Owens Cross Roads, Alabama*
[f] *University of Louisiana Monroe, Monroe, Louisiana*

(Manuscript received 17 January 2020, in final form 4 June 2020)

ABSTRACT

During November 2018–April 2019, an 11-station very high frequency (VHF) Lightning Mapping Array (LMA) was deployed to Córdoba Province, Argentina. The purpose of the LMA was validation of the Geostationary Lightning Mapper (GLM), but the deployment was coordinated with two field campaigns. The LMA observed 2.9 million flashes (≥ five sources) during 163 days, and level-1 (VHF locations), level-2 (flashes classified), and level-3 (gridded products) datasets have been made public. The network's performance allows scientifically useful analysis within 100 km when at least seven stations were active. Careful analysis beyond 100 km is also possible. The LMA dataset includes many examples of intense storms with extremely high flash rates ($>1\,s^{-1}$), electrical discharges in overshooting tops (OTs), as well as anomalously charged thunderstorms with low-altitude lightning. The modal flash altitude was 10 km, but many flashes occurred at very high altitude (15–20 km). There were also anomalous and stratiform flashes near 5–7 km in altitude. Most flashes were small ($<50\,km^2$ area). Comparisons with GLM on 14 and 20 December 2018 indicated that GLM most successfully detected larger flashes (i.e., more than 100 VHF sources), with detection efficiency (DE) up to 90%. However, GLM DE was reduced for flashes that were smaller or that occurred lower in the cloud (e.g., near 6-km altitude). GLM DE also was reduced during a period of OT electrical discharges. Overall, GLM DE was a strong function of thunderstorm evolution and the dominant characteristics of the lightning it produced.

1. Introduction

a. Background

North-central Argentina has long been recognized as home to some of the strongest thunderstorms on Earth (Zipser et al. 2006; Liu et al. 2007; Cecil and Blankenship 2012). In particular, Córdoba Province and surrounding regions frequently suffer from large hail and other forms of severe convective weather (Mezher et al. 2012; Bruick et al. 2019). This region features unique topography that includes a small mountain range called the Sierras de Córdoba (SDC), which is physically separate from the much larger Andes range located to its west (Fig. 1). The SDC interacts with the warm and moist air from the South American low-level jet (SALLJ), mechanical subsidence in the lee of the Andes, and other meteorological features to provide orographic forcing of deep, intense convection that often back builds along the terrain (Rasmussen and Houze 2011, 2016; Rasmussen et al. 2014; Bruick et al. 2019). This creates a relatively geographically confined area where convective initiation, upscale growth, and development of severe weather can occur in rapid succession, enabling a natural laboratory for studying multiple stages of convective evolution without needing to cover the

Supplemental information related to this paper is available at the Journals Online website: https://doi.org/10.1175/JTECH-D-20-0005.s1.

Corresponding author: Timothy J. Lang, timothy.j.lang@nasa.gov

DOI: 10.1175/JTECH-D-20-0005.1

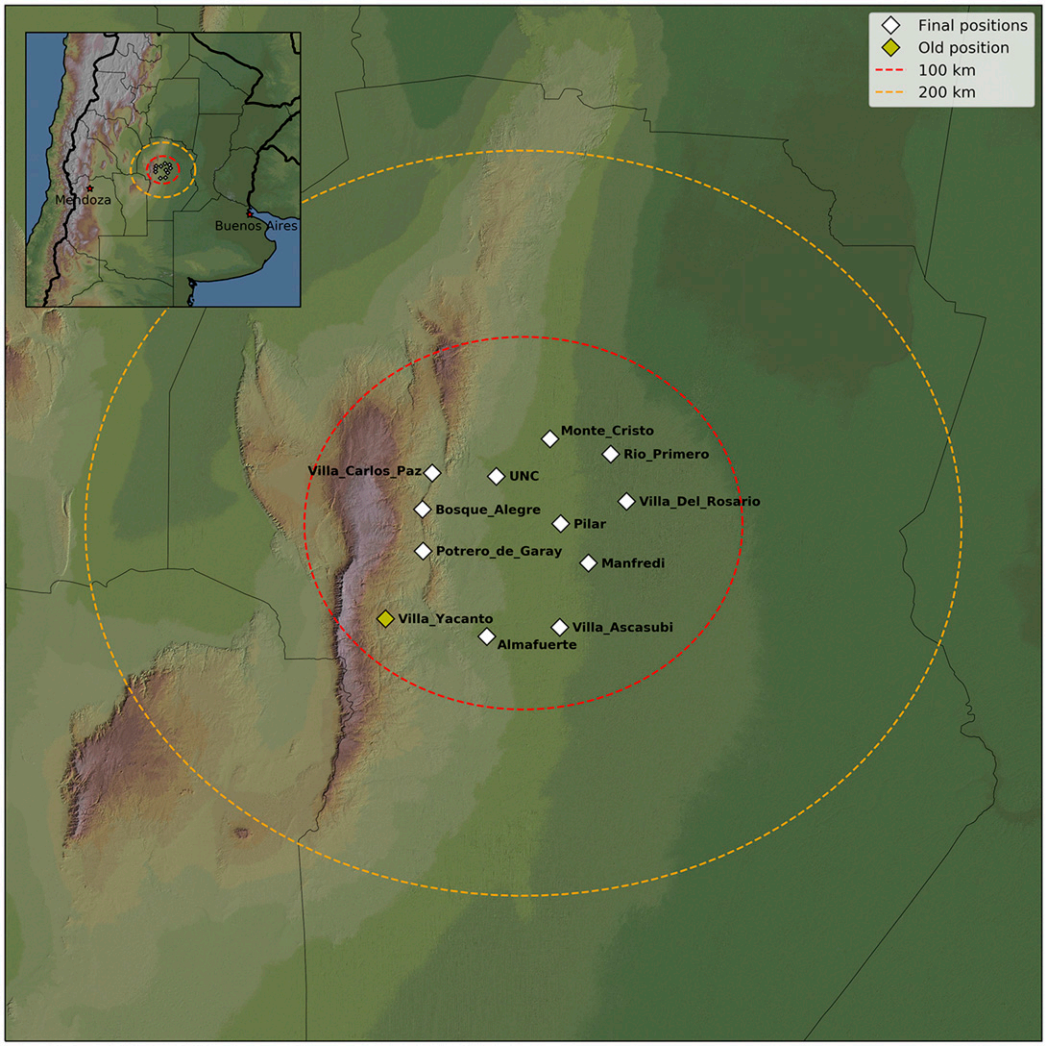

FIG. 1. Map of the RELAMPAGO LMA. Station names are listed next to their positions. The inset shows the regional context for the network.

large distances often required in, for example, the U.S. central plains.

To study the above phenomena, two coordinated international field campaigns occurred near Córdoba from late 2018 through early 2019. The Remote Sensing of Electrification, Lightning, and Mesoscale/Microscale Processes with Adaptive Ground Observations (RELAMPAGO) field campaign focused on high-impact convective weather, and the Clouds, Aerosols, and Complex Terrain Interactions (CACTI) field campaign focused on the representation of orographic clouds in atmospheric models (RELAMPAGO-CACTI 2020). The U.S. components of these field campaigns, primarily funded by the National Science Foundation (NSF; RELAMPAGO) and the Department of Energy (DOE; CACTI) in collaboration with multiple partner institutions in Argentina and Brazil, deployed several instrument platforms—including polarimetric Doppler radars, mobile soundings and surface meteorological measurements, profilers, hydrometeorological measurements, in situ aircraft, Marx meter arrays, low-frequency lightning detectors, and electric field mills—for periods ranging from a few weeks to several months.

b. The RELAMPAGO Lightning Mapping Array

Because of the high concentration of complementary instrumentation focused on deep convection and intense thunderstorms, as well as the unique and heretofore sparsely observed meteorological environment of north-central Argentina, the Geostationary Operational Environmental Satellite, R series (GOES-R), calibration/validation program funded the deployment

of an 11-station very high frequency (VHF) Lightning Mapping Array (LMA; Rison et al. 1999) from November 2018 through April 2019. The RELAMPAGO LMA was installed and operated by the National Aeronautics and Space Administration (NASA) George C. Marshall Space Flight Center (MSFC) and for a period of at least 163 days mapped lightning in three dimensions in a region that encompassed the SDC, the city of Córdoba, and surrounding areas (Fig. 1).

The primary purpose of the RELAMPAGO LMA was to produce a validation dataset for the Geostationary Lightning Mapper (GLM) on *GOES-16*, which provides operational coverage of Argentina (Goodman et al. 2013; Rudlosky et al. 2019). In particular, the deployment was intended to better understand how electrical phenomena in different regions of the world could pose potential challenges for GLM. The electrical phenomena include storms with anomalous charge structures with midlevel positive charge (from −10° to −25°C; e.g., Rust et al. 2005; Lang and Rutledge 2011; Bruning et al. 2014), storms with extremely high flash rates ($>1\,s^{-1}$) composed primarily of small flashes (e.g., Bruning and MacGorman 2013), and electrical discharges in the overshooting tops (OTs; e.g., MacGorman et al. 2017). Unfortunately, the LMA deployment did not coincide with the GLM instrument on *GOES-17*, which had a postlaunch checkout positioning near 89.5°W longitude earlier in 2018.

This paper will describe the deployment of the RELAMPAGO LMA, document data processing and quality control procedures, explain the performance of the network, describe the LMA dataset whose public release is coordinated with this study, and provide some initial scientific results and comparison with GLM. In-depth studies that combine LMA data with other RELAMPAGO-CACTI sensors, including radars and different lightning detectors, are in progress and will be reported later.

FIG. 2. Photograph of the Potrero de Garay LMA station, which was virtually identical to all other RELAMPAGO LMA stations (photograph credit: T. Lang).

2. RELAMPAGO LMA deployment

a. Overview of LMA stations

The RELAMPAGO LMA consisted of 11 stations derived from NASA MSFC's inventory. These stations were originally acquired in 2012 to support the Hydrology Cycle in the Mediterranean Experiment (HyMeX; Drobinski et al. 2014; Lang et al. 2017). They all used revision-3 (Rev3) LMA boards originally developed by the New Mexico Institute of Mining and Technology (NMT). Prior to RELAMPAGO/CACTI, the LMA station configurations were updated for easier deployment (Fig. 2). Station electronics—including the station computer, LMA board, global positioning system (GPS) card, and hard drive—were enclosed within a sealed metal box (LMA box) and placed inside a plastic storage container. A polyvinyl chloride (PVC) frame surrounded the storage container and held a 140-W solar panel and antenna mast in place using wire and zip ties. The solar panel charged two 12-V marine deep-cycle batteries inside the storage container. The weight of the batteries, LMA box, and VHF preamplifier inside the storage container secured the entire station in place. Within the antenna mast, a GPS antenna and tetrahedral VHF antenna were connected via cabling to the LMA box. The same GPS cable length was used at each station to simplify data processing. Channel 3 (60–66 MHz) was used for the vast majority of the experiment to receive signals. For a few days in November,

an unsuccessful experiment using channel 5 (76–82 MHz) was performed at one station.

The network operated continuously during November–April. Station and network performance were monitored through the use of CloudGate modems (card installed in each LMA box, with Yagi directional antenna mounted on the mast), which enabled Secure Socket Shell (SSH) access to each station via third generation (3G) cellular connections. However, bandwidth costs prohibited real-time data processing. Instead, regularly executed scripts sent station health data, and the SSH connectivity was used for troubleshooting. The Short-Term Prediction Research and Transition Center (SPoRT) at MSFC provided near-real-time GLM and Advanced Baseline Imager (ABI) imagery focused on the RELAMPAGO-CACTI domain, which was regularly checked for storms when intensive observing periods (IOPs) for RELAMPAGO were not occurring (after mid-December). When storm cases were noted in other datasets, typically 10–20 min of representative level-0 data from each available station were downloaded and processed to level-1 VHF source locations (see below), to ensure that normal mapping of lightning was continuing to occur.

b. *Network installation and operation*

In late 2017, a predeployment site survey was performed with the assistance of the Facultad de Matemática, Astronomía y Física, Universidad Nacional de Córdoba (FAMAF-UNC). As a result of that site survey, as well as network performance modeling (Chmielewski and Bruning 2016), LMA stations ended up being hosted on a mixture of publicly and privately held sites, with a mixture of background noise levels (from −65 dBm down to −90 dBm). Station spacing was deliberately spread out across a diameter of ~100 km and multiple sites were placed at higher elevations (up to 1275 m MSL) to improve network range and vertical resolution following Koshak et al. (2018). Based on predeployment modeling, horizontal source location accuracy was estimated to be < 100 m, and vertical location accuracy < 1 km, within 100-km range of the network (Thomas et al. 2004; Chmielewski and Bruning 2016).

Installation commenced with the first station on 24 October 2018 and ended with the eleventh station installed three weeks later on 14 November. Six stations were operational by 8 November, enabling minimal operational status and accurate GPS locations at this time. Between 19 and 23 November one station was moved from Villa Yacanto (a radio-noisy DOE site) to another site at Potrero de Garay (see Fig. 1), which unfortunately ended up about as noisy (approximately −65 dBm). Elevated background noise also impacted sites at Manfredi and Villa Ascasubi, although for the latter only at night. Conversely, sites at Villa Del Rosario and Almafuerte became significantly less noisy (at least 10 dBm decrease) after collocated lightning sensors (in particular electric field meters) were removed in mid-December. The average noise throughout the network was approximately −74 dBm, somewhat higher than expected based on the original site survey, and likely 5–10 dBm higher than U.S. networks such as the north Alabama LMA (Koshak et al. 2004).

Figure 3 shows a time series of the maximum number of stations available on any given day during the project. Primary challenges faced by the deployment included wind damage to the PVC superstructure, malfunctioning LMA boards, and power issues. Occasional postmaintenance mistakes with incorrectly reconnecting cables caused multiday outages at two sites. Insect infestations that impeded routine maintenance but did not otherwise affect data also impacted two sites. Wind damage generally occurred when stations had insufficient duct tape, zip ties, wire, and glue, which led to separation of PVC joints that was rapidly repaired during follow-up site visits. The LMA board malfunctioning, which caused otherwise good GPS input data to become garbled because of flipped bits, temporarily affected multiple sites. The most common cause was frequent diurnally based thermal cycling of the boards, which led the socketed plastic-leaded chip carrier (PLCC) chips on the Rev3 boards to become loose. Reseating the chips often fixed this problem; however, at sites at which it did not the LMA boards were eventually replaced. Potrero de Garay experienced a combined hard drive and LMA board failure that led to most (although not all) of its data being lost between 8 December 2018 and 12 February 2019. Power issues became more common late in the deployment, with multiple stations often shutting down overnight starting in April, as a result of aging batteries and seasonally low sun angles. After 19 April 2019, there were no longer at least six stations operating reliably throughout the day and night, so this was the effective end of the LMA deployment. The network was disassembled and shipped back to MSFC by early May 2019. Logistical lessons learned from the deployment are discussed in section 6b.

3. LMA data processing and quality control

a. *Overview of data processing*

As mentioned previously, the first step for creating an LMA dataset is to process level-0 trigger data from each available station to level-1 VHF source locations. This step was performed for the period from 8 November 2018 through 19 April 2019 using the "lma_analysis" software developed by NMT. A VHF source was located

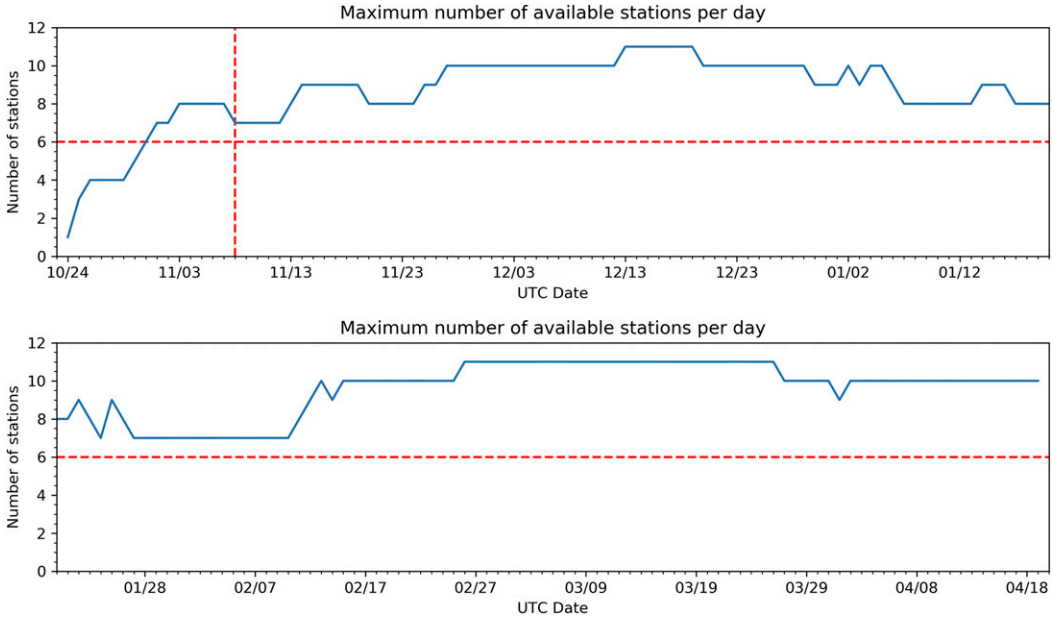

FIG. 3. Time series of daily maximum RELAMPAGO LMA station availability. The vertical red dashed line indicates the start date for viable data (8 Nov 2018), and the horizontal red dashed lines indicate the minimum six stations needed for location solutions.

if at least six stations detected it and the χ^2 goodness-of-fit parameter was 5 or less. The level-1 processing made use of the time-of-arrival method, originally developed by Proctor (1971) and then later refined by various researchers (Koshak and Solakiewicz 1996; Rison et al. 1999; Koshak et al. 2004; Thomas et al. 2004).

After this, level-2 processing occurred, wherein VHF sources were automatically sorted into flashes. This was done using the "lmatools" software (Bruning 2015) following the method of Fuchs et al. (2016). This approach uses the open-source density-based spatial clustering of applications with noise (DBSCAN) clustering algorithm, with the following criteria: no more than 150 ms or 3 km between successive sources in a flash, and flashes were limited to 3-s maximum duration. These are fairly typical criteria (e.g., MacGorman et al. 2008; Fuchs et al. 2015). Although flashes can last longer than 3 s (e.g., Lang et al. 2017), this is rare. Inspection of the longest-duration flashes in the RELAMPAGO dataset (~2.6 s) did not indicate obvious flash-splitting artifacts.

Gridded level-3 products, such as flash extent density (FED) and flash energy, were created after level-2 processing was completed. These products were developed following the method of Bruning and MacGorman (2013) as implemented in the lmatools software (Bruning 2015).

b. *Effects of station availability on data quality*

Because the number of stations available varied significantly during the project, this would be expected to affect source detection (and thus flash detection) efficiency (Thomas et al. 2004; Chmielewski and Bruning 2016; Koshak et al. 2018). To gauge the impact of this using real data, a sensitivity study was performed using 10 min of data on 14 December 2018, for which 11 stations were available and contributing to level-1 solutions. This case, which featured an intense mesoscale convective system (MCS) centrally located within the network, was processed assuming 6–11 stations were available (Fig. 4). Stations were removed from the analysis in the order in which they failed during December 2018–February 2019. Then flash processing was run using variable assumptions about χ^2 and minimum number of sources per flash. Table 1 shows the results for total flash rate versus number of stations available. Combining Fig. 4 and Table 1, for only six stations detected sources are reduced by ~97% relative to 11 stations, and it is not possible to fully recover either the total flash rate or FED seen with the full 11 stations, no matter how generous the χ^2 or points per flash criteria get. However, with at least 7 stations, ~20% of the 11 station sources are available, and it is possible to get within ~5% of the 11-station flash rates. In addition, although peak FED magnitudes are not recoverable with only seven stations, it is possible to recover the approximate spatial envelope containing nonzero FED within 100 km of network center. Each additional station improves the results while enabling more restrictive assumptions about χ^2 and points per flash.

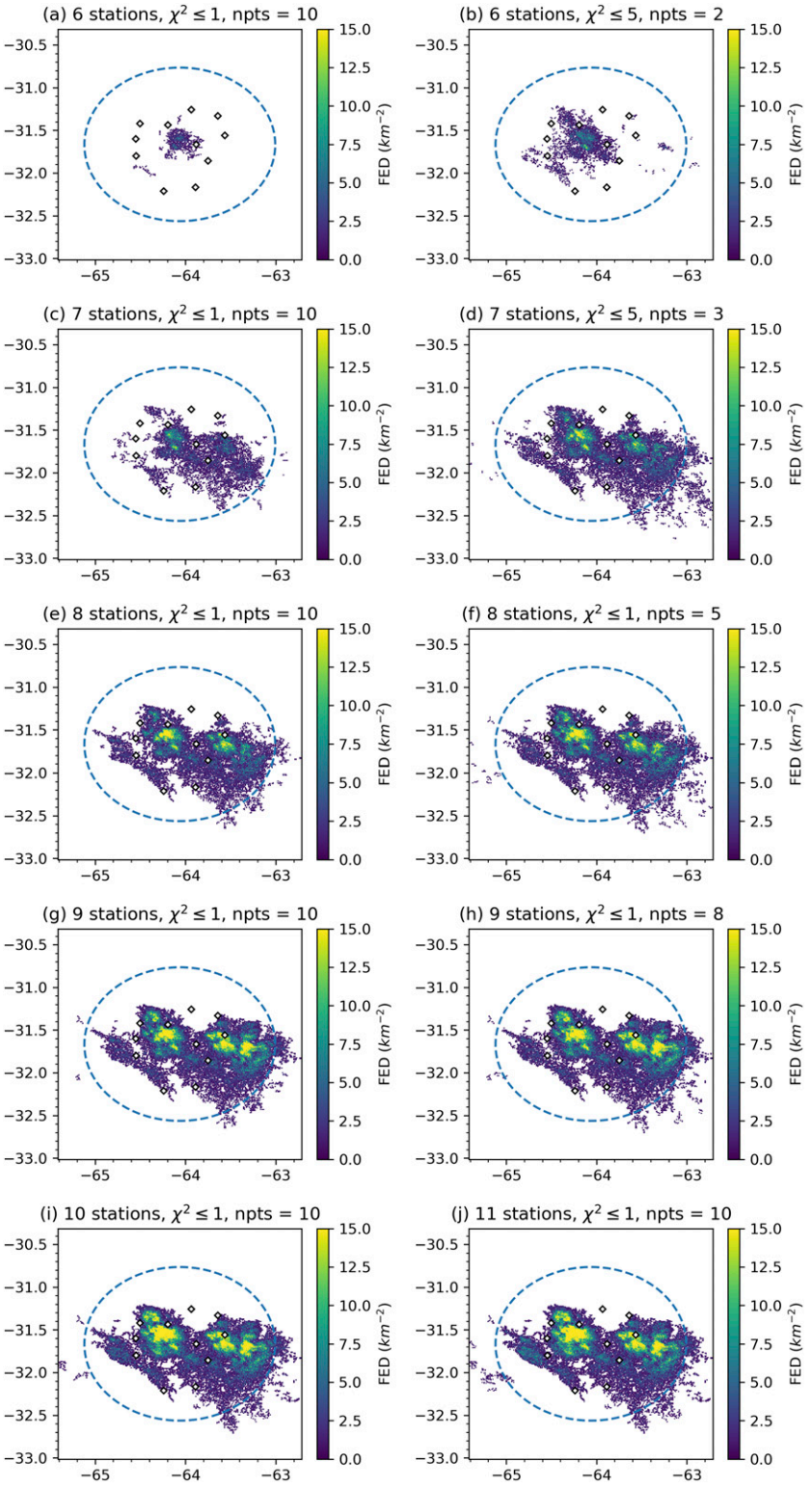

FIG. 4. FED for 0330–0340 UTC 14 Dec 2018, processed using different assumptions. Station locations are indicated by the open diamonds, and the range ring is 100 km. Shown are (a) 6 stations, $\chi^2 \leq 1$, and 10 points per flash; (b) 6 stations, $\chi^2 \leq 5$, and 2 points per flash; (c) 7 stations, $\chi^2 \leq 1$, and 10 points per flash; (d) 7 stations, $\chi^2 \leq 5$, and 3 points per flash; (e) 8 stations, $\chi^2 \leq 1$, and 10 points per flash; (f) 8 stations, $\chi^2 \leq 1$, and 5 points per flash; (g) 9 stations, $\chi^2 \leq 1$, and 10 points per flash; (h) 9 stations, $\chi^2 \leq 1$, and 8 points per flash; (i) 10 stations, $\chi^2 \leq 1$, and 10 points per flash; and (j) 11 stations, $\chi^2 \leq 1$, and 10 points per flash.

TABLE 1. Total flash counts (within 100 km of network center) for 10 min of LMA data starting at 0330 UTC 14 Dec 2018, depending on how many stations are available and how the data are processed (npts = minimum threshold for number of LMA sources per flash). Also shown are the percentages of sources detected within 100 km, relative to the 11-station scenario.

	Percent of sources relative to 11 stations ($\chi^2 \leq 5$)	Unadjusted flash count ($\chi^2 \leq 1$; npts = 10)	Adjusted flash count	Adjustment
6 stations	3.3	96	679	$\chi^2 \leq 5$; npts = 2
7 stations	20.2	709	3980	$\chi^2 \leq 5$; npts = 3
8 stations	48.9	1899	4019	$\chi^2 \leq 1$; npts = 5
9 stations	76.6	3293	4083	$\chi^2 \leq 1$; npts = 8
10 stations	95.8	4060	—	—
11 stations	100.0	4207	—	—

To further explore the influence of station availability on detection efficiency, the integrated VHF source densities for 14 active lightning days with 7–8 operational stations, and 14 active lightning days with 10–11 operational stations, are compared in Fig. 5. While there was a drop-off in source density with fewer stations (cf. Figs. 5a and 5b), it was not dramatic and the source ratio of fewer to more stations almost always was above 10% within 100 km (Fig. 5c). Indeed, the presence of especially active storms in certain regions on the 7–8-station days even led to ratios exceeding 100%, most notably in the SW of the network, as well as north beyond 100-km range (Fig. 5c). Within 100 km, the total number of sources detected during 7–8-station cases (21.8 million) was ~40% of the 10–11-station number (55.1 million), which is within the range expected from the independent analysis presented in Table 1 (20%–50%).

The average number of stations available during the campaign was roughly eight or nine (Fig. 3). Thus, as a compromise for the version-1 data release (discussed below), level-2 and level-3 products were developed using a χ^2 of 5 and number of sources per flash of five. This allowed 7-station cases to provide more scientifically useful results while still preventing 10–11-station cases from having the least restrictive criteria. However, care should be taken when comparing flash rates between cases with different numbers of available stations, or when station availability varied during a case. In particular, when station availability dropped to six stations, retrieved flash rates decreased dramatically no matter what. An example is provided for the 25 January 2019 case (Fig. S1 in the online supplemental material), which generally had seven stations or more. There were temporary outages (LMA board malfunction) when station availability dropped to six (around 2000 UTC and again around 2100 UTC), leading to steep declines in total flash rate, but rates immediately recovered when the seventh station returned to service.

A more complex processing method (e.g., dynamically varying flash criteria based on station availability) may be attempted for later LMA dataset versions, if they are produced. In addition, data users are welcome to reprocess the level-2 and level-3 data for specific cases with their preferred criteria, since the processing

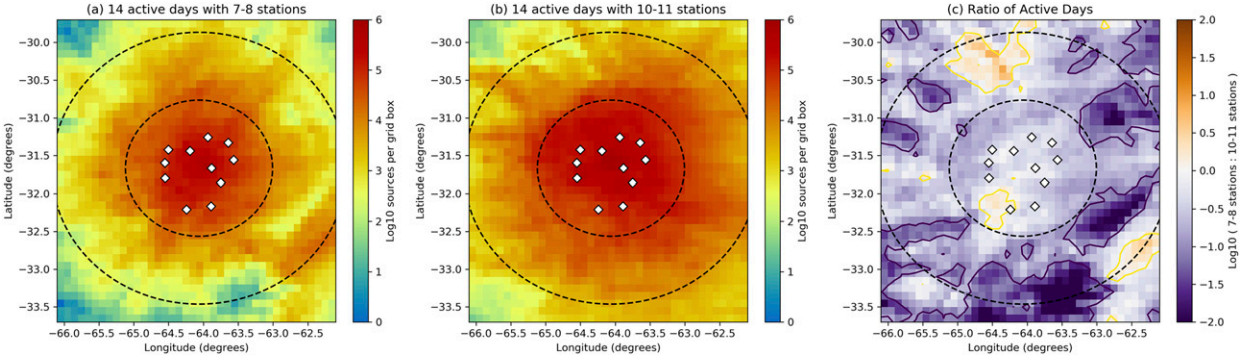

FIG. 5. (a) Integrated LMA source density for 14 active days that featured almost exclusively 7–8 available stations (22–26 Jan, 29 Jan–2 Feb, and 8–11 Feb). (b) Integrated LMA source density for 14 active days that featured almost exclusively 10–11 available stations (13–14 Dec, 17–18 Dec, 22–24 Feb, 4 Mar, 7–8 Mar, and 14–17 Mar). (c) Ratio of the densities plotted in (a) and (b). The purple line contours indicate where the 7–8 station days have fewer than 10% of the sources observed during the 10–11 station days. Also shown in each subplot are station locations (open diamonds) and 100-km range rings.

TABLE 2. Summary of RELAMPAGO LMA level-1–3 data product information.

	Level 1	Level 2	Level 3
Format	ASCII	HDF5	netCDF4
Core product	LMA sources	LMA flashes	Gridded flash characteristics
Spatial domain	All detected sources	All detected sources and flashes	±200-km horizontal; 0–20-km vertical
Temporal domain	10 min	10 min	10 min
Grid resolution	—	—	$1 \times 1 \times 1\ \text{km}^3 \times 1$ min
Key variables	Time, lat, lon, alt, χ^2, no. of stations, and power	All level-1 source variables, plus flash identification, 3D location, time, area, duration, no. of sources, and energy	2D and 3D: FED, initiation density, footprint, energy, no. of sources, and flash size
Thresholding	≥6 stations per source; $\chi^2 \leq 5$	≥6 stations per source; $\chi^2 \leq 5$; 5 sources per flash	≥6 stations per source; $\chi^2 \leq 5$; 5 sources per flash

tools are open source. Level-1 data would not need reprocessing.

4. RELAMPAGO LMA public dataset

The version-1 RELAMPAGO LMA dataset consists of level-1–3 data from 8 November 2018 through 19 April 2019. Appropriate documentation is also provided. The release is through the NASA Global Hydrology Resource Center (GHRC) Distributed Active Archive Center (DAAC; Lang 2020).

The documentation included in the release provides detailed explanations of the different datasets. Summary information is provided in Table 2. All levels of data are provided in files with 10-min increments, following the usual LMA community standard for data reporting. Level-1 data are in the standard American Standard Code for Information Interchange (ASCII) format for LMA data that has been used by the community for about two decades. Level-2 data contain a copy of the VHF source data provided in the level-1 products, as well as flash identification and metrics (area, duration, etc.), and are in version-5 Hierarchical Data Format (HDF5). Note that level-1 and level-2 data are not restricted in range from the network; that is, if a source/flash was detected it is included in these products. Available open-source software to ingest and process level-1 and level-2 data includes lmatools (Bruning 2015).

Level-3 data are in version-4 Network Common Data Form (netCDF4) and are gridded in either two or three

TABLE 3. Top 20 RELAMPAGO lightning days, for flashes with at least five sources ($\chi^2 \leq 5$) and whose centroids were within 100 km of the network center.

Rank	Date	Total flashes	Notes
1	25 Jan 2019	167 174	MCS developed within network
2	14 Dec 2018	162 276	Severe MCS in center of network
3	4 Mar 2019	116 888	MCS moved south to north through network
4	2 Jan 2019	97 863	High-flash-rate multicell storms
5	24 Feb 2019	93 115	Series of multicells moved west to east in network
6	22 Feb 2019	90 617	Intense high-flash-rate cells near network center
7	10 Feb 2019	74 360	Intense cells with possible lightning hole
8	11 Feb 2019	72 495	MCS moved through network to northeast
9	11 Nov 2018	67 177	Daylong series of discrete storms
10	12 Nov 2018	64 517	Daylong series of discrete storms
11	8 Mar 2019	56 528	MCS moving through network to northeast
12	9 Jan 2019	55 938	Multiple discrete cells in network
13	23 Jan 2019	51 256	High-flash-rate multicells
14	26 Jan 2019	46 306	MCS with frequent stratiform lightning
15	29 Jan 2019	45 207	Multiple mountain-based thunderstorms
16	27 Dec 2018	43 310	High-flash-rate multicells
17	6 Jan 2019	40 193	Round of strong convection and then stratiform lightning
18	31 Mar 2019	33 707	Supercell plus other multicellular storms
19	8 Feb 2019	27 157	Mountain-based convection
20	9 Feb 2019	26 478	Strong multicell developing from previous-day storms

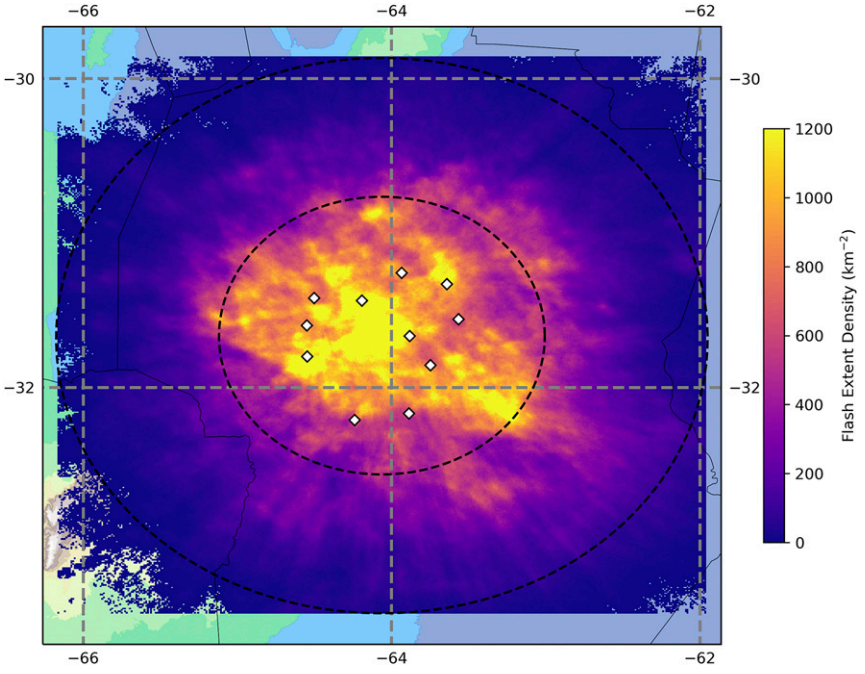

FIG. 6. Integrated FED from 8 Nov 2018 through 19 Apr 2019. Latitude/longitude grid lines are shown, along with station locations (open diamonds) and 100-km range rings. FED was only gridded to ±200 km from network center.

spatial dimensions, depending on the variable. Each level-3 file contains a different variable. These grids are fixed in 1-km Cartesian spacing in all spatial dimensions. In the horizontal plane this is relative to network center (approximately 31.7°S, 64.1°W), and in the vertical direction it is relative to the 1984 World Geodetic System (WGS84) standard spheroid surface at network center. The grids extend ±200 km from the horizontal center and 20 km in the vertical direction. In time the grids are binned in 1-min intervals (i.e., ten 1-min time bins per 10-min file). See Table 2 and the level-3 documentation at GHRC (Lang 2020) for more information. These netCDF4 level-3 files are readable by a large variety of open- and closed-source software packages and contain sufficient metadata to be fully self-describing.

5. Initial scientific results

a. Lightning climatology

The LMA deployment was very successful in measuring lightning. Of the 163 days of the deployment for which data are available, at least one lightning flash was detected within 100 km of the LMA on 76 days. This meant that 46.6% of the days featured nearby lightning, with a grand total of 1 683 073 flashes detected within 100 km (based on the flash criteria summarized in Table 2). The top 20 most active days are shown in Table 3. All months except April 2019 are represented in this list. The list also spans a variety of storm modes and numbers of available stations (Fig. 3). For example, the most active day, 25 January 2019, had a maximum of nine different operational stations, but generally no more than eight were active at any one time because of transient LMA board malfunctions (recall the discussion about supplemental Fig. S1). Four days with a maximum of seven active stations (11–12 November 2019, and 10–11 February 2019) are represented in the top 10. Meanwhile, the second-most active day, 14 December 2018, had as many as 11 stations operational. Thus, reduced network capacity did not necessarily impose a barrier on the detection of large quantities of lightning within 100 km.

The integrated map of FED for the entire deployment is shown in Fig. 6. This map was derived from the 2D level-3 FED products, which are limited to ±200 km from network center (Table 2). While the highest values of FED are observed within the network, large values (>1000 km^{-2}) are observed as distantly as 100 km. Beyond that range, a significant drop-off in FED occurred. There was also a drop-off in FED beyond a northwest–southeast line near the southwest portion of the 100-km range ring. This was likely due to SDC

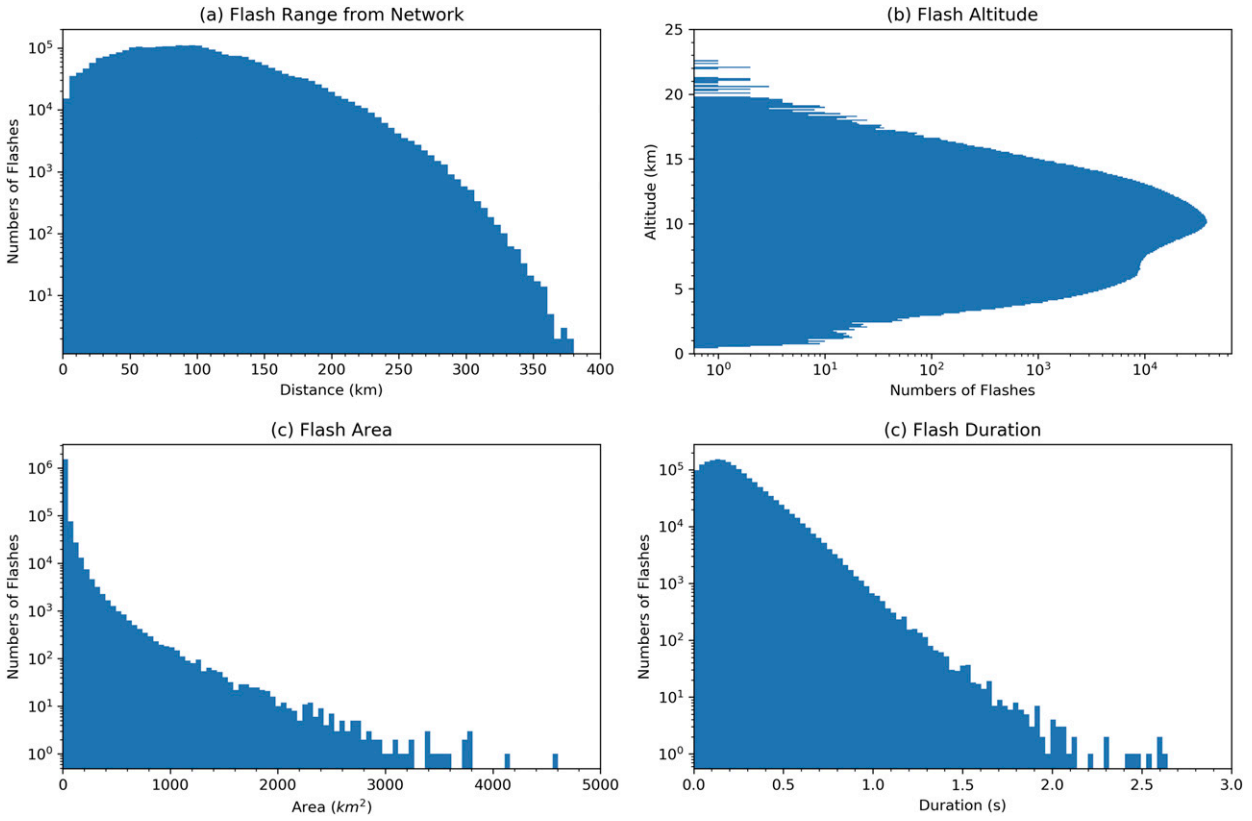

FIG. 7. (a) Histogram of flash centroid distances from network center. (b) Histogram of flash centroid altitudes within 100-km range. (c) Histogram of flash areas for flash centroids within 100-km range. (d) Histogram of flash durations for flash centroids within 100-km range. Data are from 8 Nov 2018 through 19 Apr 2019.

orography (Fig. 1), which may have caused line-of-sight detection issues as well as controlled the preferred locations and routes for orographically generated convection. Flash frequency versus range is shown in Fig. 7a. The maximum frequency of flashes was observed within 50–100-km range. However, 1.286 million flashes still were observed beyond 100 km. The most distantly observed flash was 379 km from network center.

Flash centroid altitude distribution is shown in Fig. 7b. To focus on data with the best expected altitude errors (<1 km), only flashes within 100 km of network center are shown. The mode of the distribution was at 10 km. This was similar to the vertical distribution of flashes found in northern Alabama by Fuchs and Rutledge (2018). The secondary peak at 6 km was likely due to a combination of both anomalously charged storms (Lang and Rutledge 2011) and stratiform lightning activity occurring within the network, as both of these produce flash centroids at lower altitudes. An example of an anomalous storm in Argentina will be shown in the next section.

The flash area histogram is shown in Fig. 7c. Area was estimated using the convex hull method of Bruning and MacGorman (2013). Approximately 1.5 million flashes (of 1.68 million within 100 km, or ~90%) are contained within the smallest bin in this distribution, 0–50 km^2. This is smaller than the area of a GLM pixel (Goodman et al. 2013), which illustrates the challenge that GLM could have in observing most flashes detected and classified by the LMA. Less than 1300 flashes (of 1.68 million, or ~0.1%) were observed with areas exceeding 1000 km^2. Approximately 68% of the flashes contained more than 10 VHF sources, and 16% contained more than 100 sources (not shown because the distribution is similar to flash area). The flash duration distribution is shown in Fig. 7d. The overwhelming majority (93%) of lightning flashes observed by the LMA lasted less than 500 ms. In addition, the shape of the duration distribution, with the thin tail ending around 2.6 s, supports the processing choice of the 3-s threshold for maximum flash duration.

The diurnal cycle of lightning is shown in Fig. 8. Interestingly, there were two observed peaks in lightning occurrence, one near 5 p.m. local time and one near midnight local. This dual convective mode reflected typical afternoon convection that tended to weaken

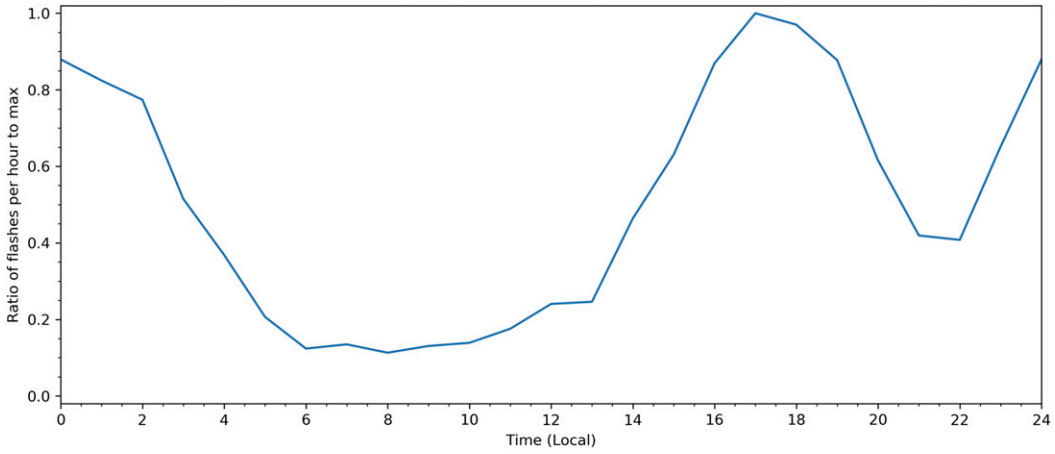

FIG. 8. Normalized diurnal cycle of hourly lightning flash rate within 100 km of the LMA center, from 8 Nov 2018 through 19 Apr 2019.

after sunset, before overnight redevelopment. These peaks approximately agreed with the satellite-based hailstorm climatology for this region of Bruick et al. (2019), particularly for medium-probability hailstorms (see their Fig. 4). The afternoon peak is well explained by diurnal, orographic forcing near the SDC, while a convective peak near midnight has been observed near this region in other datasets (Rasmussen et al. 2014; Piersante 2017). This overnight peak likely relates to upscale growth in convection driven by the SALLJ interacting with the SDC (Rasmussen and Houze 2011).

b. Comparison with GLM

1) OVERVIEW

As mentioned in the introduction, there are certain modes of lightning that may pose a challenge for GLM to characterize accurately. This initial comparison between GLM and the RELAMPAGO LMA will focus on three possible challenges: 1) extremely high flash rates ($>1\,s^{-1}$), 2) electrical discharges in OTs, and 3) anomalously charged thunderstorms that likely feature predominantly positive charge in the midlevels (from $-10°$ to $-25°C$). Issue 1 generally leads to the repeated occurrence of spatially small flashes in the same region of the storm, that is, flashes whose optical signatures may only affect one GLM pixel (Rudlosky et al. 2019). In addition, the flashes' optical energy outputs may be small (Zhang and Cummins 2020). Issue 2 also likely results in spatially small flashes occurring in a confined region. Moreover, the physical characteristics of OT electrical discharges are poorly understood (MacGorman et al. 2017), and thus their optical output is uncertain. Potentially mitigating this, however, is that the activity is literally occurring in the top of the thunderstorm, where cloud optical thickness is minimized. Issue 3 leads to lightning occurring deeper within the cloud, likely within regions of heavy precipitation (Fuchs and Rutledge 2018). This leads to a ''quenching'' effect wherein the light from flashes does not sufficiently escape the optically thick portions of the cloud and thus may not get detected by GLM.

The net result is that GLM may significantly underdetect these three lightning phenomena (small flashes, OT electrical discharges, deep flashes) relative to the LMA. Thus, the LMA can be used to document the extent of the underdetection for each phenomenon, and perhaps provide guidance on how to account for it. Conversely, GLM can be used to document range limitations of the LMA, thereby providing an independent check on its performance. These issues will be examined using two case studies.

Level-2 GLM Lightning Cluster Flash Algorithm (LCFA) data (Rudlosky et al. 2019) and level-2 LMA flash data were reprojected and interpolated to a common 10-km horizontal resolution fixed grid, following the method of Bruning et al. (2019) as implemented in ''glmtools'' (Bruning 2019) and lmatools (Bruning 2015). Two-dimensional FED was computed for both datasets on this common grid. Because the cases analyzed had 10–11 LMA stations available, the minimum VHF sources per flash threshold was raised to 10. This would tend to reduce LMA flash rates and FED relative to the 5-point threshold used elsewhere in this study but should also limit the impact of VHF noise (which generally increases with additional stations) on flash statistics.

In addition, a flash-matching algorithm was applied to the original level-2 GLM and LMA data. The algorithm

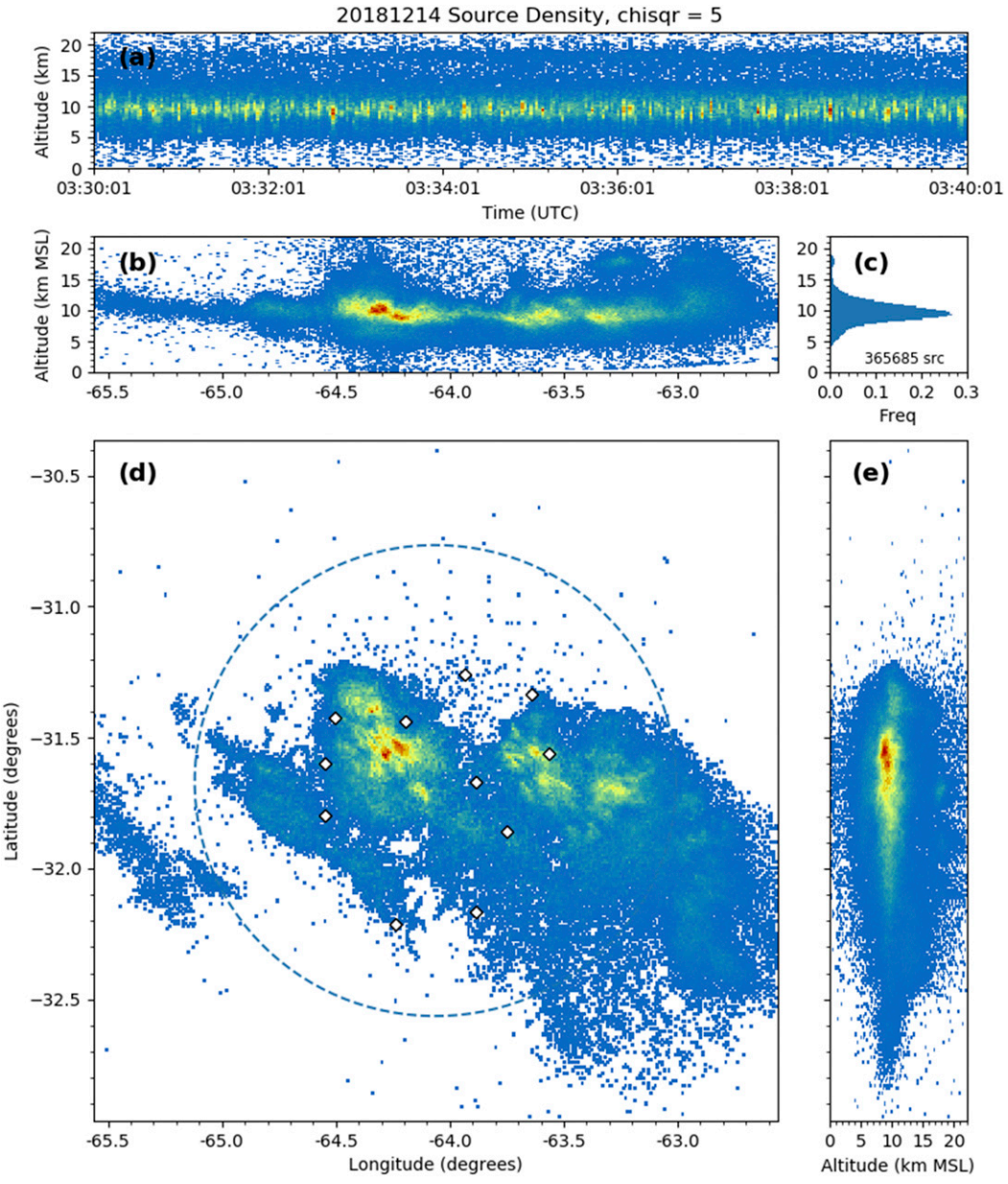

FIG. 9. "XLMA"-style plot for LMA source density for 0330–0340 UTC 14 Dec 2018: (a) Time–height. (b) Longitude–height. (c) Normalized vertical distribution of sources, with total number of sources observed. (d) Plan view. Also shown are LMA station locations (open diamonds) and the 100-km range ring. (e) Latitude–height. In all subplots except (c), the density color scale is relative and unique to that particular subplot—blue is the lowest density of sources and red is the highest.

used simple and arbitrary thresholds (<25-km centroid distance and ±500-ms start time offset) because the goal of this analysis is to understand how GLM detection efficiency (DE) varies as flash and thunderstorm characteristics evolve, rather than whether GLM meets its DE specifications in Argentinian thunderstorms (this will be addressed in future studies). While matching LMA to GLM flashes, the analysis allowed for multiple LMA flashes to correspond to a single GLM flash. This was to account for observational differences between the radio-frequency-based (LMA) and optically based (GLM) instruments (i.e., that which appears spatially coherent as a single optical flash at cloud top may in fact be represented in cloud by distinctly separate VHF-mapped flashes, because of diffuse scattering of light).

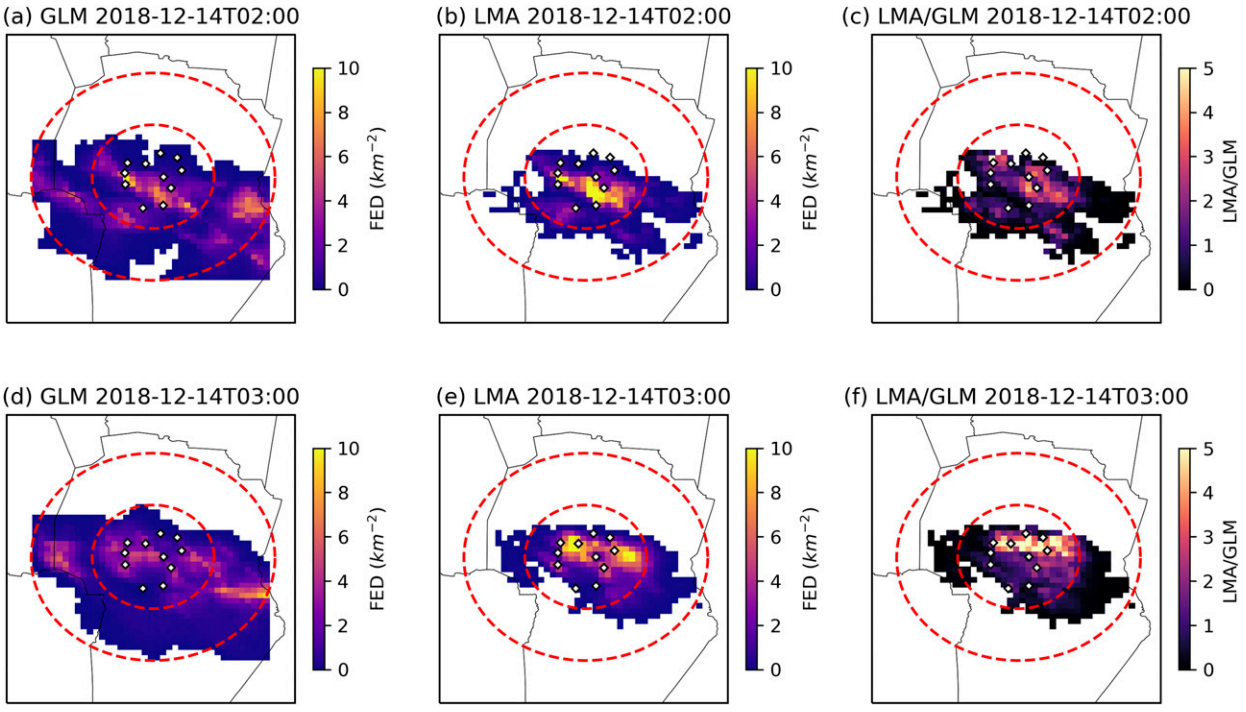

FIG. 10. (a),(d) GLM FED; (b),(e) LMA FED; and (c),(f) ratio of LMA FED to GLM FED for (top) the 0200 UTC hour and (bottom) the 0300 UTC hour on 14 Dec 2018. LMA and GLM have been interpolated to a matched 10-km grid that extends ±200 km from the LMA center in each direction. Also shown in all panels are LMA station locations (open diamonds) and 100-km range rings. No ratio was calculated where the LMA FED was 0.

2) 14 DECEMBER 2018

The 14 December 2018 case was a severe MCS that featured very high flash rates (flash rate within 100 km peaked near 600 min^{-1}) as well as OT electrical discharges. LMA source density for 0330–0340 UTC (Fig. 9) was representative of a time period when electrical discharges in the OT occurred above 15 km. The OT activity was evidently associated with an intense updraft in the western storm core at −63.25° longitude during this time (Fig. 9b). OT electrical discharges were most frequent during the 0300 UTC hour. In Fig. 10, comparisons of integrated hourly FED between GLM and the LMA are shown for the 0200 UTC hour (which featured rapid intensification of LMA flash rate; Figs. 10a–c) as well as the 0300 UTC hour (Figs. 10d–f). During these time periods, the LMA indicated two major regions of high FED within 100-km range, one in the west half of the network and one in the east (Figs. 10b,e). LMA FED typically exceeded GLM FED by as much as a factor of 5 in these convective regions (Figs. 10c,f). However, a notable exception was the western convection during the 0200 UTC hour. The FED peak between the Bosque Alegre and Potrero de Garay stations was comparable between the two instruments (Figs. 10a,b). The FED comparison also indicated the range limitations of the LMA—beyond 100 km there were large areas where LMA FED was below GLM FED (i.e., ratio < 1; Figs. 10c,f).

Time series of DE of GLM relative to the LMA are shown in Fig. 11a. This analysis examined two different thresholds for the minimum number of points per LMA flash (10 and 100). For 10 points per LMA flash, the DE was typically 70% or greater, save for very early in the storm's lifetime (<0150 UTC) and again in the middle of the 0300 UTC hour (when OT electrical discharges were noted). DE increased after 0530 UTC, eventually reaching > 90% by the time the decaying storm left the 100-km range limit for comparison. GLM DE was 10%–20% larger on average when considering larger flashes with a minimum of 100 LMA sources. However, this DE also declined during the OT period.

One potential reason why GLM DE was so variable during the storm may have been because time series of flash rates and sizes showed an anticorrelation between average LMA flash size and flash rate (Fig. 11b). That is, periods of high LMA flash rate also corresponded to times when flash sizes (as measured by average points per flash) were small, and thus more difficult for GLM to detect (Zhang and Cummins 2020). (Note: In developing

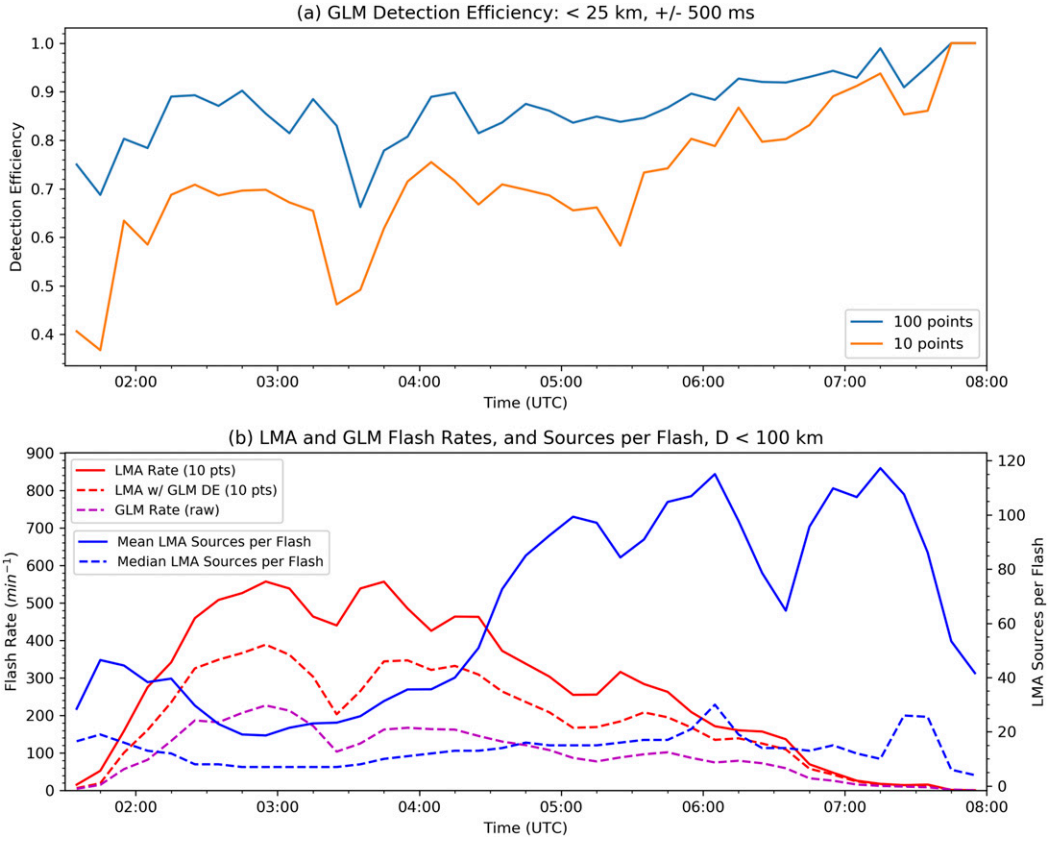

FIG. 11. (a) Time series of GLM DE within 100 km of the LMA on 14 Dec 2018, relative to LMA flashes with 10 or 100 minimum points. (b) Time series of LMA flash rate, LMA flash rate adjusted by the estimated time-varying GLM DE, and the raw GLM flash rate, all within 100 km of the LMA. Also shown are median and mean LMA sources per flash.

the flash size curves, the 10-source threshold for LMA flash classification was relaxed to 3 sources, as this enabled identification of possible times when the 10-point threshold was significantly impacting LMA flash rates.) LMA flash rate also declined during the OT period (near 0330 UTC). One possible explanation for this is that smaller discharges were occurring in the OT and elsewhere that were represented by LMA sources (Fig. 9) but not classified as flashes by the LMA flash algorithm (due to the 10-point threshold; MacGorman et al. 2017). This would effectively decrease LMA flash rate even as source activity grew within the OT and elsewhere (Fig. 12a).

3) 20 DECEMBER 2018

The main storm of interest on 20 December 2018 was an intense cell that developed and moved through the northern half of the LMA (Fig. 13). This was an active storm (peak flash rate ~250 min^{-1}), but a significant fraction of the LMA sources occurred between 5 and 10 km in the vertical in the main storm, suggesting an anomalous electrical structure (Wiens et al. 2005; Lang and Rutledge 2011; Bruning et al. 2014; Fuchs and Rutledge 2018). Matched-grid GLM and LMA FED are shown for the 2000 and 2100 UTC hours in Fig. 14. During both hours, the LMA saw significantly greater FED in the northeast anomalous storm (FED ratio > 5; Figs. 14c,f). Similar to 14 December (Fig. 10), GLM tended to observe greater FED beyond 100-km range.

Time series of the GLM DE, flash rate, and flash size during approximately 2000–2200 UTC were dominated by the strongest storm in the northern portion of the network (Fig. 15). GLM DE was overall significantly worse than the 14 December case (Fig. 11), with 10-source DE as low as ~30%, and 100-source DE as low as ~60% during the analysis period (Fig. 15a). The time of lowest DE, especially for the largest flashes, corresponded well with the ~2045–2115 UTC time period when LMA source density was maximized near 6-km altitude (Fig. 12b). These results suggest that flash altitude was impacting GLM DE via quenching of the optical signal when flashes occurred deeper in the cloud (Fuchs and Rutledge 2018). Mean LMA flash size peaks around 2015 and 2315 UTC (Fig. 15b) corresponded with relative increases in 10-point GLM DE but were evidently anticorrelated with LMA

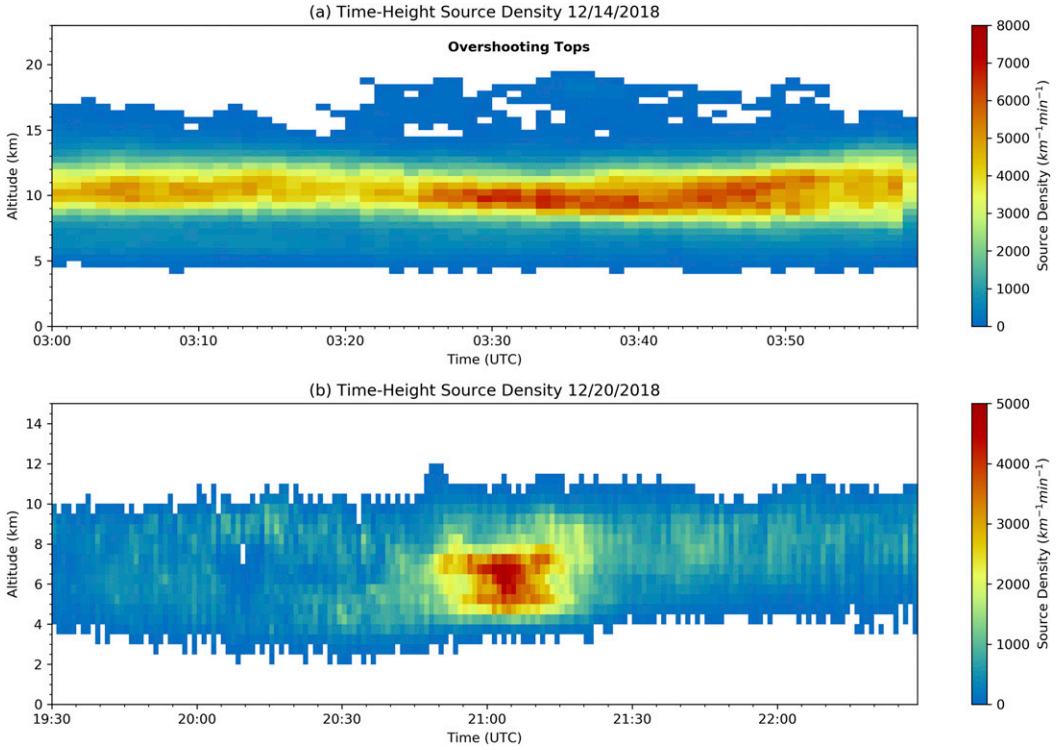

FIG. 12. Time–height LMA source density for the domain within 100 km of network center for (a) 14 and (b) 20 Dec 2018. The approximate time and location of OT electrical activity is labeled.

flash rate, which was maximized around 2115 UTC. This was similar to the results seen on 14 December 2018, when smaller flash sizes led to reduced GLM DE. Thus, variations in both flash altitude and flash size appeared to affect GLM DE on 20 December 2018.

In both case studies (14 and 20 December 2018), GLM did observe increases in flash rate when the LMA observed major flash rate spikes, but the magnitude of the increase was suppressed relative to the LMA. This was true even if the GLM DE was corrected based on comparison with the LMA (e.g., Figs. 11 and 15). This was evidently due to fluctuations in DE that corresponded in time with changes in average flash size, the occurrence of small-scale OT electrical discharges, and/or lowering of the altitude where lightning was occurring (Figs. 11 and 15). This supports the hypothesis described in section 5b(1) that GLM has a more difficult time detecting lightning flashes when they grow smaller or move lower in altitude within a cloud (Fuchs and Rutledge 2018; Zhang and Cummins 2020).

6. Summary and conclusions

a. Scientific lessons learned

The RELAMPAGO LMA deployment was a success, with millions of flashes detected over a period of 5+ months. A large variety of thunderstorms were observed, from mountain-forced airmass storms, to severe supercells, to large MCSs, and many modes in between. This LMA dataset will be of potential interest to any researchers studying intense convection. In particular, the dataset contains numerous examples of electrical activity in OTs, as well as some examples of anomalously charged storms with low-altitude lightning.

Overall, the network's performance allows scientifically useful analysis within 100 km when at least seven stations were active. Data users should be able to trust flash products, in particular lightning trends in storms, in almost all situations within that range (with the caveat that dropping to six active stations led to a significant decrease in performance; supplemental Fig. S1). Moreover, useful analysis beyond 100 km is also possible, but the data user is cautioned to consider reduced LMA DE at these distances.

Initial comparisons with GLM indicated that the satellite instrument most successfully detected larger flashes (e.g., > 100 VHF sources per LMA flash). Detection efficiency of such flashes could exceed 90%. However, GLM DE was also a strong function of thunderstorm evolution and the dominant characteristics of lightning it was producing. For example, GLM DE was reduced to as low as ~30% during certain portions of the 14 and

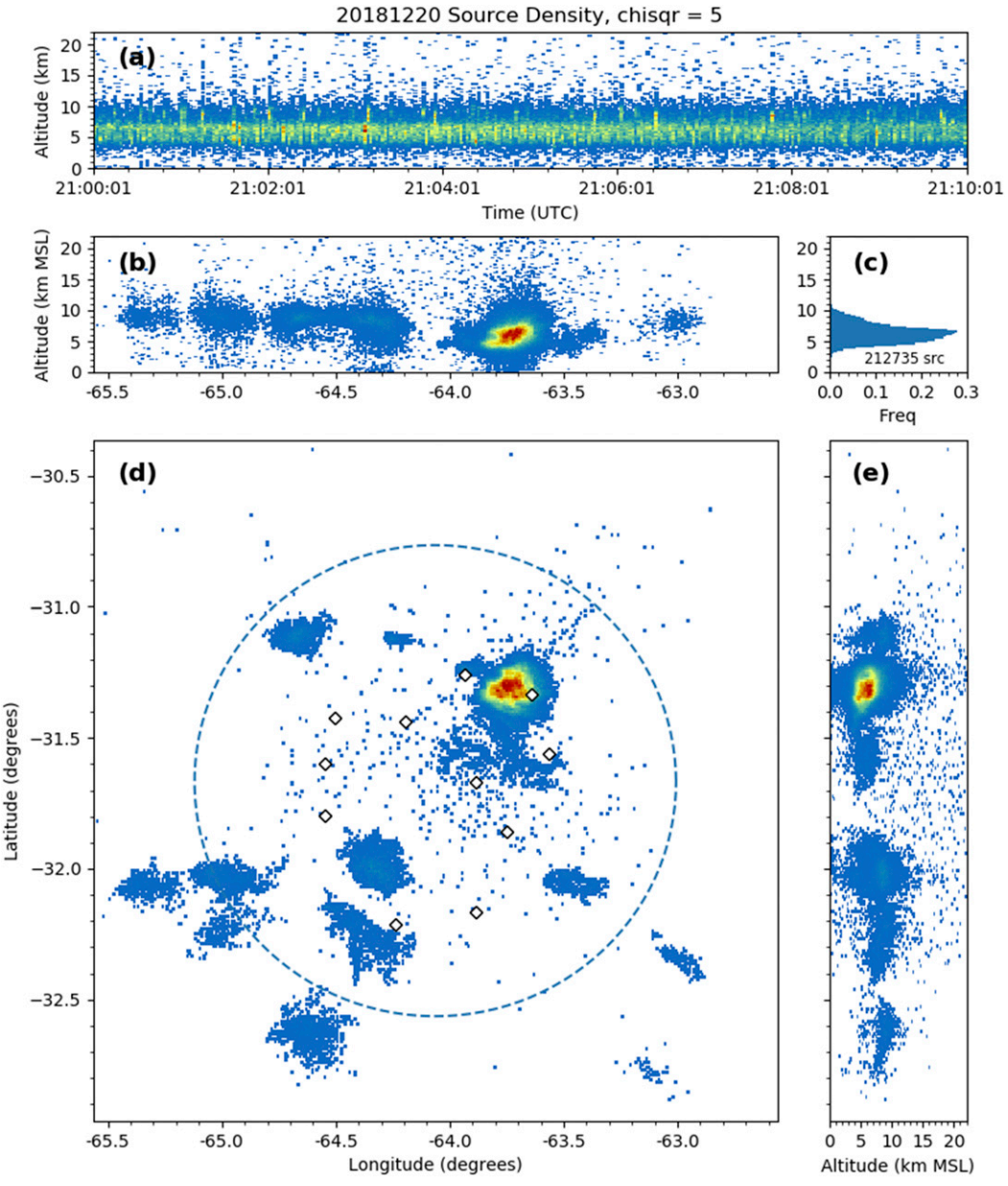

FIG. 13. As in Fig. 9, but for 2100–2110 UTC 20 Dec 2018.

20 December thunderstorm lifetimes, particularly when LMA flash size (as measured by sources per flash) trended smaller, or when flashes occurred deeper in the storm—such as when 20 December exhibited an anomalous electrical structure. These time periods preferentially occurred coincident with the highest LMA flash rates within the two storms. This tended to dampen raw GLM flash rate trends—GLM observed the increases in flash rate, but they were not as dynamic as the LMA trends. This has implications for operational end users of GLM data, who might wish to use these data for severe weather nowcasting. Such stakeholders will need to consider this caveat when interpreting GLM flash rate trends in intense storms.

b. Logistical lessons learned

One logistical lesson learned from the deployment is that, while the PVC frames and antenna mast overall worked well, they also greatly benefitted from extra securing of the pipe joints via generous use of duct tape, glue, zip ties, etc. Stations that received wind damage and then were thoroughly repaired did not experience

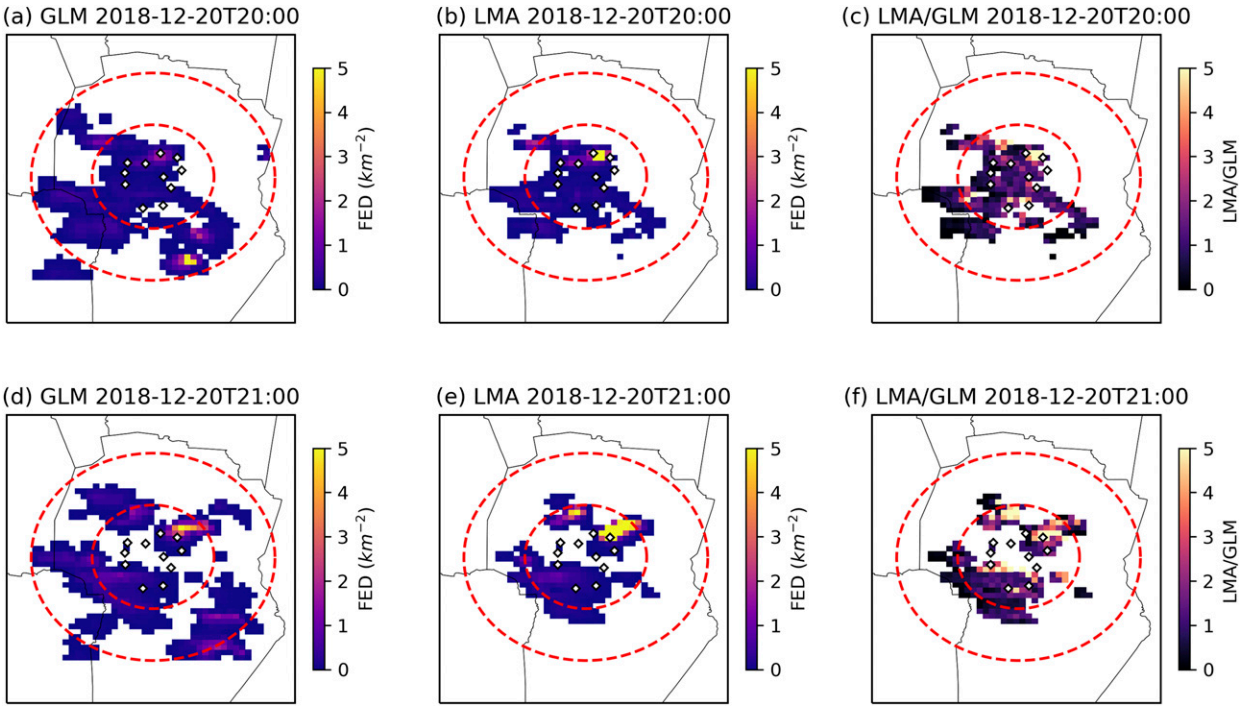

FIG. 14. As in Fig. 10, but for (a)–(c) the 2000 UTC hour and (d)–(f) the 2100 UTC hour on 20 Dec 2018.

damage again (note that wind damage never caused a station outage). Late-season operations would have benefitted from a third battery or second solar panel at the most problematic sites, due to limited solar charging. Rev3 LMA boards should be thoroughly vetted and PLCC chips prophylactically reseated before future deployments. (Later versions of LMA boards discontinued the use of PLCC chips.)

However, the most important lesson of the deployment is that having a willing, knowledgeable, and helpful in-country partner like FAMAF-UNC was absolutely critical. The RELAMPAGO LMA deployment would have been a failure without FAMAF-UNC's advocacy and assistance. FAMAF-UNC made the difference with shipping and customs assistance, site selection and its role as landowner liaison, and occasional site visits to fix issues that would crop up between NASA trips to Argentina.

Acknowledgments. RELAMPAGO LMA stations were generously hosted by the following individuals and organizations: Maria Mercedes Cáceres, Center for Severe Weather Research (CSWR), Colegio Instituto Bachillerato Agrotecnico (IBAT) San Jose, Colegio Instituto Provincial de Educación Agrotécnica (IPEA), Instituto Nacional de Tecnología Agropecuaria (INTA), Raúl Mari, Milton Pecorari, Jorge Picatto, Observatorio Astronómico Bosque Alegre, Luis Orangio, Servicio Meteorológico Nacional (SMN), Claudia Tomaselli, FAMAF-UNC, and the U.S. Department of Energy (DOE). In addition, the following individuals and organizations are thanked for their significant contributions to the scientific and/or logistical components of the LMA deployment: Leigh Anderson, Eric Bruning, Dan Cecil, Vanna Chmielewski, David Corredor, Carlos De La Vega, Lisa Dorsett, Harald Edens, Carlos Marcelo Garcia, Betsy Goldemen, Mirta Iriondo, Gilbert Kirkham, Bill Koshak, Joy Marich, NASA Global Hydrology Resource Center (GHRC), NASA MSFC Shipping and Receiving, NASA Short-Term Prediction Research and Transition Center (SPoRT), National Center for Atmospheric Research (NCAR), Steve Nesbitt, Walt Petersen, Bill Rison, Dan Rodeheffer, Paola Salio, The Serena Group, Leigh Sinclair, Gail Skofronick-Jackson, Michael Solomon, Geoffrey Stano, the U.S. Embassy in Argentina, and Brad Zavodsky. Major funding for the RELAMPAGO LMA came from the NOAA GOES-R Program, with additional support from the NASA Lightning Imaging Sensor (LIS) project. Coauthor Goodman acknowledges support from NASA Grant 80NSSC18K1689. Coauthors Bitzer, Burchfield, Carey, Medina, and Wingo acknowledge research funding from NASA MSFC Award NNM11AA01A and NSF Award AGS 1661785. Coauthor Melo was supported by the NSF Research Experience for Undergraduates (REU) program. Coauthor Deierling also was supported by

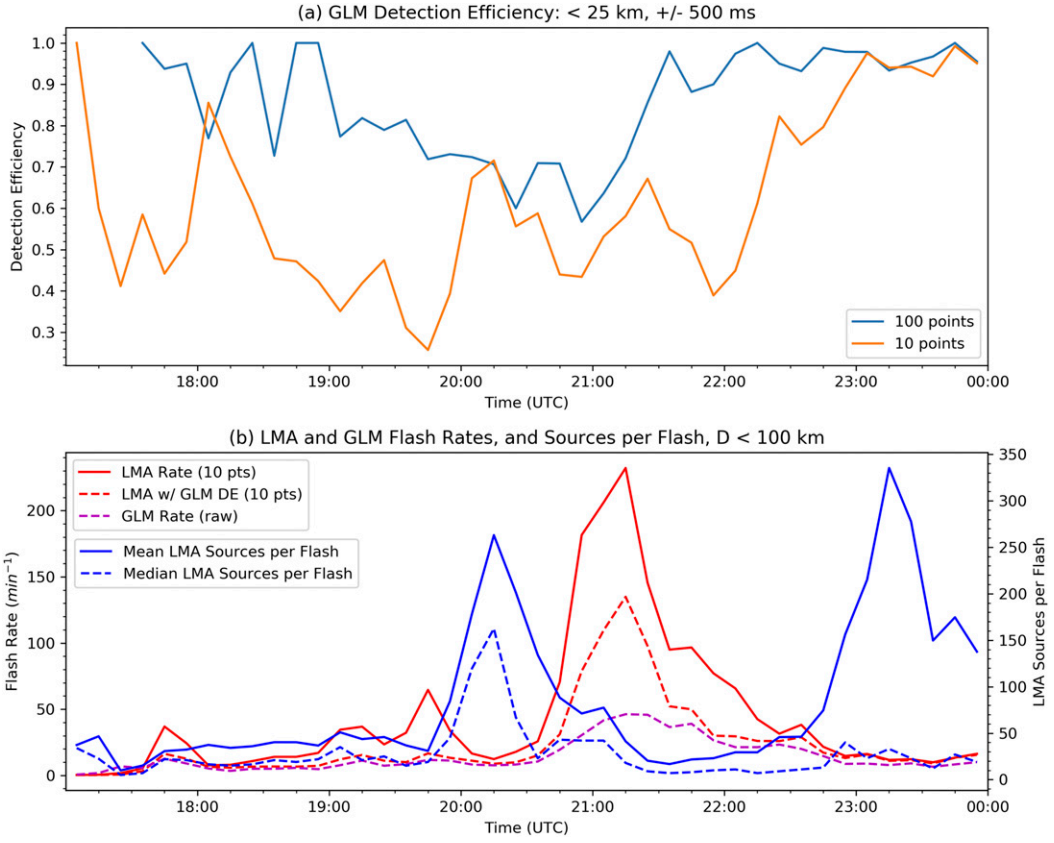

FIG. 15. As in Fig. 11, but on 20 Dec 2018.

NSF. The views, opinions, and findings in this report are those of the authors and should not be construed as an official NASA or U.S. government position, policy, or decision.

Data availability statement. LMA data are available from NASA (https://doi.org/10.5067/RELAMPAGO/LMA/DATA101). GLM data are available from NOAA (https://www.avl.class.noaa.gov/saa/products/welcome).

REFERENCES

Bruick, Z. S., K. L. Rasmussen, and D. J. Cecil, 2019: Subtropical South American hailstorm characteristics and environments. *Mon. Wea. Rev.*, **147**, 4289–4304, https://doi.org/10.1175/MWR-D-19-0011.1.

Bruning, E. C., 2015: lmatools: lmatools-v0.5z-stable, version v0.5z. Zenodo, https://doi.org/10.5281/zenodo.32510.

——, 2019: deeplycloudy/glmtools: glmtools release to accompany publication, version v0.5.0. Zenodo, https://doi.org/10.5281/zenodo.2648658.

——, and D. R. MacGorman, 2013: Theory and observations of controls on lightning flash size spectra. *J. Atmos. Sci.*, **70**, 4012–4029, https://doi.org/10.1175/JAS-D-12-0289.1.

——, S. A. Weiss, and K. M. Calhoun, 2014: Continuous variability in thunderstorm primary electrification and an evaluation of inverted-polarity terminology. *Atmos. Res.*, **135–136**, 274–284, https://doi.org/10.1016/j.atmosres.2012.10.009.

——, and Coauthors, 2019: Meteorological imagery for the Geostationary Lightning Mapper. *J. Geophys. Res. Atmos.*, **124**, 14 285–14 309, https://doi.org/10.1029/2019JD030874.

Cecil, D. J., and C. B. Blankenship, 2012: Toward a global climatology of severe hailstorms as estimated by satellite passive microwave imagers. *J. Climate*, **25**, 687–703, https://doi.org/10.1175/JCLI-D-11-00130.1.

Chmielewski, V. C., and E. C. Bruning, 2016: Lightning Mapping Array flash detection performance with variable receiver thresholds. *J. Geophys. Res. Atmos.*, **121**, 8600–8614, https://doi.org/10.1002/2016JD025159.

Drobinski, P., and Coauthors, 2014: HyMeX: A 10-year multidisciplinary program on the Mediterranean water cycle. *Bull. Amer. Meteor. Soc.*, **95**, 1063–1082, https://doi.org/10.1175/BAMS-D-12-00242.1.

Fuchs, B. R., and S. A. Rutledge, 2018: Investigation of lightning flash locations in isolated convection using LMA observations. *J. Geophys. Res. Atmos.*, **123**, 6158–6174, https://doi.org/10.1002/2017JD027569.

——, and Coauthors, 2015: Environmental controls on storm intensity and charge structure in multiple regions of the continental United States. *J. Geophys. Res. Atmos.*, **120**, 6575–6596, https://doi.org/10.1002/2015JD023271.

——, E. C. Bruning, S. A. Rutledge, L. D. Carey, P. R. Krehbiel, and W. Rison, 2016: Climatological analyses of LMA data with an open-source lightning clustering algorithm. *J. Geophys. Res. Atmos.*, **121**, 8625–8648, https://doi.org/10.1002/2015JD024663.

Goodman, S. J., and Coauthors, 2013: The GOES-R Geostationary Lightning Mapper (GLM). *Atmos. Res.*, **125–126**, 34–49, https://doi.org/10.1016/j.atmosres.2013.01.006.

Koshak, W. J., and R. J. Solakiewicz, 1996: On the retrieval of lightning radio sources from the time-of-arrival data. *J. Geophys. Res.*, **101**, 26 631–26 639, https://doi.org/10.1029/96JD01618.

——, and Coauthors, 2004: North Alabama Lightning Mapping Array (LMA): VHF source retrieval algorithm and error analyses. *J. Atmos. Oceanic Technol.*, **21**, 543–558, https://doi.org/10.1175/1520-0426(2004)021<0543:NALMAL>2.0.CO;2.

——, D. M. Mach, and P. M. Bitzer, 2018: Mitigating VHF lightning source retrieval errors. *J. Atmos. Oceanic Technol.*, **35**, 1033–1052, https://doi.org/10.1175/JTECH-D-17-0041.1.

Lang, T., 2020: Remote Sensing of Electrification, Lightning, and Mesoscale/Microscale Processes with Adaptive Ground Observations (RELAMPAGO) Lightning Mapping Array (LMA), level 1, 2, and 3 datasets. NASA Global Hydrology Resource Center DAAC, accessed 16 July 2019, https://doi.org/10.5067/RELAMPAGO/LMA/DATA101.

——, and S. A. Rutledge, 2011: A framework for the statistical analysis of large radar and lightning datasets: Results from STEPS 2000. *Mon. Wea. Rev.*, **139**, 2536–2551, https://doi.org/10.1175/MWR-D-10-05000.1.

——, and Coauthors, 2017: WMO world record lightning extremes: Longest reported flash distance and longest reported flash duration. *Bull. Amer. Meteor. Soc.*, **98**, 1153–1168, https://doi.org/10.1175/BAMS-D-16-0061.1.

Liu, C., E. J. Zipser, and S. W. Nesbitt, 2007: Global distribution of tropical deep convection: Different perspectives from TRMM infrared and radar data. *J. Climate*, **20**, 489–503, https://doi.org/10.1175/JCLI4023.1.

MacGorman, D. R., and Coauthors, 2008: TELEX: The Thunderstorm Electrification and Lightning Experiment. *Bull. Amer. Meteor. Soc.*, **89**, 997–1014, https://doi.org/10.1175/2007BAMS2352.1.

——, M. S. Elliott, and E. DiGangi, 2017: Electrical discharges in the overshooting tops of thunderstorms. *J. Geophys. Res. Atmos.*, **122**, 2929–2957, https://doi.org/10.1002/2016JD025933.

Mezher, R. N., M. Doyle, and V. Barros, 2012: Climatology of hail in Argentina. *Atmos. Res.*, **114–115**, 70–82, https://doi.org/10.1016/j.atmosres.2012.05.020.

Piersante, J., 2017: Characteristics of hail events near the Sierras de Córdoba, Argentina. SOARS Paper, 20 pp., https://opensky.ucar.edu/islandora/object/manuscripts%3A955/datastream/PDF/view.

Proctor, D. E., 1971: A hyperbolic system for obtaining VHF radio pictures of lightning. *J. Geophys. Res.*, **76**, 1478–1489, https://doi.org/10.1029/JC076i006p01478.

Rasmussen, K. L., and R. A. Houze Jr., 2011: Orogenic convection in subtropical South America as seen by the TRMM satellite. *Mon. Wea. Rev.*, **139**, 2399–2420, https://doi.org/10.1175/MWR-D-10-05006.1.

——, and ——, 2016: Convective initiation near the Andes in subtropical South America. *Mon. Wea. Rev.*, **144**, 2351–2374, https://doi.org/10.1175/MWR-D-15-0058.1.

——, M. D. Zuluaga, and R. A. Houze Jr., 2014: Severe convection and lightning in subtropical South America. *Geophys. Res. Lett.*, **41**, 7359–7366, https://doi.org/10.1002/2014GL061767.

RELAMPAGO-CACTI, 2020: RELAMPAGO-CACTI. Google, https://sites.google.com/illinois.edu/relampago/home.

Rison, W., R. Thomas, P. Krehbiel, T. Hamlin, and J. Harlin, 1999: A GPS-based three-dimensional lightning mapping system: Initial observations in central New Mexico. *Geophys. Res. Lett.*, **26**, 3573–3576, https://doi.org/10.1029/1999GL010856.

Rudlosky, S. D., S. J. Goodman, K. S. Virts, and E. C. Bruning, 2019: Initial Geostationary Lightning Mapper observations. *Geophys. Res. Lett.*, **46**, 1097–1104, https://doi.org/10.1029/2018GL081052.

Rust, W. D., and Coauthors, 2005: Inverted-polarity electrical structures in thunderstorms in the Severe Thunderstorm Electrification and Precipitation Study (STEPS). *Atmos. Res.*, **76**, 247–271, https://doi.org/10.1016/j.atmosres.2004.11.029.

Thomas, R. J., P. R. Krehbiel, W. Rison, S. J. Hunyady, W. P. Winn, T. Hamlin, and J. Harlin, 2004: Accuracy of the Lightning Mapping Array. *J. Geophys. Res.*, **109**, D14207, https://doi.org/10.1029/2004JD004549.

Wiens, K. C., S. A. Rutledge, and S. A. Tessendorf, 2005: The 29 June 2000 supercell observed during STEPS. Part II: Lightning and charge structure. *J. Atmos. Sci.*, **62**, 4151–4177, https://doi.org/10.1175/JAS3615.1.

Zhang, D., and K. L. Cummins, 2020: Time evolution of satellite-based optical properties in lightning flashes, and its impact on GLM flash detection. *J. Geophys. Res. Atmos.*, **125**, e2019JD032024, https://doi.org/10.1029/2019JD032024.

Zipser, E. J., D. J. Cecil, C. Liu, S. W. Nesbitt, and D. P. Yorty, 2006: Where are the most intense thunderstorms on Earth? *Bull. Amer. Meteor. Soc.*, **87**, 1057–1072, https://doi.org/10.1175/BAMS-87-8-1057.